

# Photon-sparse microscopy: visible light imaging using infrared illumination

REUBEN S. ASPDEN,<sup>1</sup> NATHAN R. GEMMELL,<sup>2</sup> PETER A. MORRIS,<sup>1</sup> DANIEL S. TASCA,<sup>1,7</sup> LENA MERTENS,<sup>1</sup> MICHAEL G. TANNER,<sup>3,8</sup> ROBERT A. KIRKWOOD,<sup>3</sup> ALESSANDRO RUGGERI,<sup>4</sup> ALBERTO TOSI,<sup>4</sup> ROBERT W. BOYD,<sup>5,6</sup> GERALD S. BULLER,<sup>2</sup> ROBERT H. HADFIELD,<sup>3</sup> AND MILES J. PADGETT<sup>1,\*</sup>

<sup>1</sup>SUPA, School of Physics and Astronomy, University of Glasgow, Glasgow, G12 8QQ, UK

<sup>2</sup>SUPA, School of Engineering & Physical Sciences, Heriot-Watt University, Edinburgh, EH14 4AS, UK

<sup>3</sup>SUPA, School of Engineering, University of Glasgow, Glasgow, G12 8QQ, UK

<sup>4</sup>Dipartimento di Elettronica, Informazione e Bioingegneria Politecnico di Milano, Piazza Leonardo da Vinci 32, 20133 Milano, Italy

<sup>5</sup>Department of Physics, University of Ottawa, Ottawa, Ontario, Canada

<sup>6</sup>The Institute of Optics and Department of Physics and Astronomy, University of Rochester, Rochester, New York 14627, USA

<sup>7</sup>Current address: Instituto de Física, Universidade Federal do Rio de Janeiro, Caixa-Postal 68528, Rio de Janeiro, RJ 21941-972, Brazil

<sup>8</sup>Current address: SUPA, School of Engineering & Physical Sciences, Heriot-Watt University, Edinburgh, EH14 4AS, UK

\*Corresponding author: miles.padgett@glasgow.ac.uk

Received 26 June 2015; revised 15 October 2015; accepted 29 October 2015 (Doc. ID 243868); published 10 December 2015

Conventional imaging systems rely upon illumination light that is scattered or transmitted by the object and subsequently imaged. Ghost-imaging systems based on parametric down-conversion use twin beams of position-correlated signal and idler photons. One beam illuminates an object while the image information is recovered from a second beam that has never interacted with the object. In this Letter, we report on a camera-based ghost imaging system where the correlated photons have significantly different wavelengths. Infrared photons at 1550 nm wavelength illuminate the object and are detected by an InGaAs/InP single-photon avalanche diode. The image data are recorded from the coincidentally detected, position-correlated, visible photons at a wavelength of 460 nm using a highly efficient, low-noise, photon-counting camera. The efficient transfer of the image information from infrared illumination to visible detection wavelengths and the ability to count single photons allows the acquisition of an image while illuminating the object with an optical power density of only  $100 \text{ pJ cm}^{-2} \text{ s}^{-1}$ . This wavelength-transforming ghost-imaging technique has potential for the imaging of light-sensitive specimens or where covert operation is desired. © 2015 Optical Society of America

**OCIS codes:** (110.0180) Microscopy; (110.3080) Infrared imaging; (230.7405) Wavelength conversion devices.

<http://dx.doi.org/10.1364/OPTICA.2.001049>

Low-light-level imaging at infrared wavelengths has many applications within both the technological and biological sectors. These applications span covert security systems, the imaging of light-sensitive biological samples, and imaging within semiconductor devices. However, given that the majority of

single-photon-sensitive, large-format detector arrays are silicon-based and therefore ineffective at wavelengths greater than  $1 \mu\text{m}$ , the technological difficulties with such applications are readily apparent: crafting a camera with high quantum efficiency and low noise at infrared wavelengths is difficult and expensive.

In this Letter, we circumvent the lack of infrared cameras that combine low-noise with single-photon sensitivity by performing the imaging using the so-called “ghost imaging” method. This method utilizes the spatial correlations between photons in the two output beams, signal and idler, generated through the spontaneous parametric down-conversion (SPDC) process [1].

In the 1990s, it was shown how the correlations between photons generated through SPDC could be utilized to create imaging systems [2,3]. These ghost-imaging systems rely on the strong position correlations between the beams of signal and idler photons that are produced by the SPDC process [4]. In a ghost-imaging system a transmissive object is placed in the idler beam and the transmitted photons are measured using a single-element, heralding detector. The use of a single-element detector means that measurements of photons that probe the object reveal no spatial information. In parallel to these measurements of the idler photons, a scanning single-element detector measures the corresponding signal photons—but since these signal photons do not interact with the object, again no image is formed. However, although the data from either detector on its own does not reveal an image, the correlation between the two data sets gives an image of the object. It should be noted that while ghost imaging based on parametric down-conversion is not reliant on quantum entanglement, the implicit entanglement within down-conversion provides a simple and practical source of spatially correlated photons. It has also been shown that a form of ghost imaging is possible with classical light [4–6], albeit using higher light levels where classical correlations persist even in the presence of shot noise. However, ghost imaging based on parametric down-conversion uses correlations

between individual photon pairs, and hence has unique attributes in ultra-low-light imaging. With one exception [7], in all ghost-imaging systems based on parametric down-conversion, the signal and idler have the same (degenerate) or similar wavelengths [8–10].

From a practical point of view, forming an image with light that does not directly interact with the object sounds useful. However, although the signal photons striking the position-sensitive detector have never interacted with the object, the object is still subject to illumination by an equivalent number of idler photons. Until recently, all systems based on photon pairs implemented their position-recording detector by raster-scanning a single-element detector. This reliance upon scanning meant that the maximum optical efficiency of such systems could not exceed  $1/N$ , where  $N$  is the number of pixels in the image. We overcame this limitation by using a time-gated camera that could detect the position of a single photon across the full field of view of an imaging system [11,12]. However, in that work, both the signal and idler beams had the same wavelength, and hence the system did not have the wavelength-transforming capability of this present work. The present system combines the increased detection efficiency offered by a time-gated camera with the wavelength-transforming advantages of nondegenerate ghost-imaging techniques. This combination enables ultra-low illumination infrared imaging of microscopic objects using signal and idler photons with a wavelength ratio of 1:3.

High-contrast microscopy using infrared illumination has previously been achieved using structured illumination or masking and a single-pixel detector [13,14]. However, these techniques rely on measuring a small change in signal on a large background light level, and therefore require far higher illumination powers than the single-photon regime utilized in the present work. Another technique used to image with infrared illumination is wavelength upconversion. In this technique, infrared photons illuminate the object and are then converted to a visible wavelength before being detected. However, this upconversion process suffers either degraded resolution or low conversion efficiency [15–17]. In 2014, an ingenious approach to transforming wavelength between the illumination and recording light was demonstrated by Lemos *et al.* [18]. Perhaps the most exciting aspect of that experiment was the ability to form an image without an infrared detector of any type. However, the photon flux in that imaging system was maintained at a modest level so that the image was detectable above the noise floor of a conventional low-light camera.

In this Letter, we implement a camera-based, ghost-imaging approach but use signal and idler photons at dramatically different wavelengths. Infrared photons at 1550 nm wavelength illuminate/probe the object, yet the camera data is recorded from visible photons at 460 nm that are correlated in position with the infrared photons. This configuration allows for the irradiation of the object with low-energy, infrared photons while still making use of a visible-wavelength, highly sensitive camera. The single-photon sensitivity and high timing resolution of both the heralding detector and the imaging camera allows for the use of an extremely low illumination flux, of order  $\sim 10^5$  infrared photons impinging on the object per second.

A schematic of our imaging system, shown in Fig. 1, utilizes the photon pairs generated through a highly nondegenerate SPDC process giving signal and idler wavelengths of 460 and 1550 nm, respectively. The signal and idler photons are separated

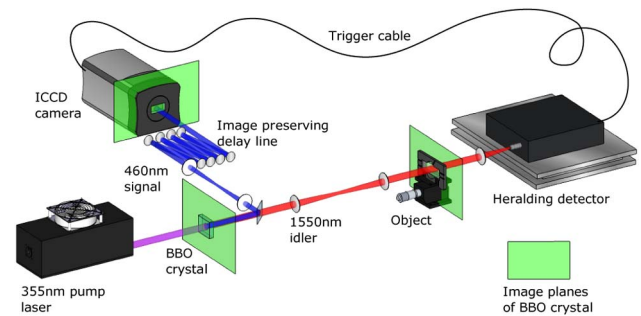


**Fig. 1.** Experimental setup. The nondegenerate SPDC process generates a visible/infrared photon pair at the BBO crystal, and these photons are split at a dichroic mirror. The infrared photon probes an object and the transmitted photons are detected by a single-element heralding detector (InGaAs/InP single-photon avalanche diode). This detection event triggers the intensifier of the ICCD camera, which detects the delayed yet spatially correlated visible photon. The recovered image of the object is the accumulation of many visible photon detections by the ICCD.

at a dichroic mirror and directed along different optical paths. The idler path contains an object that is placed in an image plane of the SPDC crystal. The idler photons that are transmitted through the object are then detected by a single-element, free-space coupled InGaAs/InP single-photon avalanche diode (SPAD) [19]. We refer to this detector as the heralding detector. In the signal path, the plane of the crystal is reimaged to a time-gated, intensified camera with a CCD detector array (ICCD). The effective magnification of our system from object plane to ICCD is  $M = 10$  (see Supplement 1). The detection of an infrared probe photon by the heralding detector is used to trigger the gate of the intensifier in the ICCD such that the signal photon that is imaged is the position-correlated visible twin of the idler photon. To ensure that we image only the correlated signal photon, we compensate for the electronic delay associated with the SPAD and the intensifier in the ICCD by a free-space, image-preserving delay line within the signal path (see Supplement 1). The average power (typically 50 mW) and repetition rate of the pump laser (100 MHz), coupled with the gating time of the intensifier (10 ns) produces a down-conversion flux such that the camera typically detects no more than one photon per triggering of the intensifier. Typically the trigger rate of the intensifier is  $\sim 10$  kHz and the exposure time (i.e., integration time) of the camera is 0.1 s, meaning that the intensifier is triggered many times per camera frame. Each triggering of the camera should, in principle, yield a measured photon. However, in practice, this efficiency is set by the optical throughput of the signal path and the quantum efficiency of the ICCD camera to approximately 7%. Although giving 50–100 photons per frame, the large number of camera pixels means there is on average much less than one photon per pixel in each frame. To each frame, we then apply our photon-counting methodology (see Supplement 1) to convert these frames into photons per pixel. We then sum the photons detected over many frames to give an accumulated image. The resulting image data is again in the form of number of detected photons per pixel. The computational overhead of data transfer means that at a frame exposure time of 0.1 s, we can acquire six frames per second.

To illustrate the wavelength-transforming capabilities of our system, we use an object formed from a polished silicon wafer onto which was patterned a microscopic gold test target

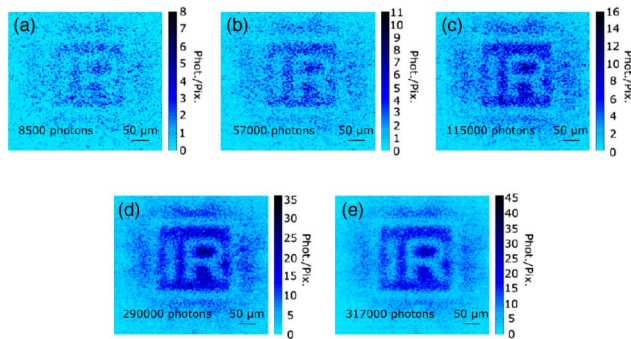


**Fig. 2.** Image of a test object. A stencil of the letter “IR” obtained in visible light by an ICCD camera, even though the object was illuminated only by infrared radiation. The object is etched into gold deposited onto a  $387\ \mu\text{m}$  thick silicon substrate. For every infrared photon that probed the object and was detected by the heralding detector, the ICCD camera was triggered to record the position-correlated visible photon. The images were formed by summing over many photon-detection events as labeled.

(created by electron beam lithography, electron beam deposition, and liftoff). The height of the letters (“IR”) to be imaged are  $120\ \mu\text{m}$ , set within a framing box of width  $160\ \mu\text{m}$ . At a wavelength of  $1550\ \text{nm}$ , the silicon is transparent whereas the gold layer is not. Note that any residual  $460\ \text{nm}$  signal photons that are in the idler path will be fully absorbed by the silicon substrate and therefore cannot trigger the heralding detector. We also note that any  $1550\ \text{nm}$  photons in the signal path will not be detectable by the ICCD camera, as the photons are outside the spectral range of the photocathode of the intensifier.

Figure 2 shows images corresponding to the accumulation of photons as more of the ICCD camera frames are summed together to recover the accumulated images. In this case, the duration of data acquisition ranged from  $30\ \text{s}$  to  $10\ \text{min}$ . Even with extremely photon-sparse images, it is possible to use reconstruction techniques to recover images of high visual quality [12] (see Supplement 1).

Two useful figures of merit for measuring the quality of an imaging system are the resolution and the contrast of the acquired images. In Fig. 3, we show long exposure images of a silicon “ $\lambda$ ” on a gold background and a gold “IR” on a silicon background. The images were acquired using the settings just detailed and a  $30\ \text{min}$  total exposure time, yielding an image contrast of  $71\%$ . The spatial resolution of the system corresponds to a point spread function of approximately  $15\ \mu\text{m}$  ( $2\sigma$ ). This spatial resolution is fundamentally limited by a combination of the strength of the spatial correlation between the down-converted signal and idler photons and the diffraction limit of the various relay optics,

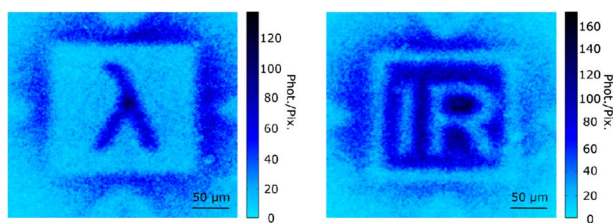


**Fig. 3.** Silicon “ $\lambda$ ” on a gold background and a gold “IR” on a silicon background. These visible images produced from the infrared illumination correspond to a total accumulation time of  $30\ \text{min}$ .

(see Supplement 1). Our understanding is that this in no way exceeds the classical limit.

The images in Fig. 2 were acquired by detection of between  $8500$  photons in image (a) and  $317,000$  photons in image (e). However, when considering low-light imaging, the number of photons detected by the camera is not the most pressing consideration. Rather, the most important characteristic is the number of photons incident on the object for the duration of the acquisition. We calculate this by measuring the number of photons detected by the heralding detector with no object present. Given the detection efficiency of this heralding detector, we can infer the number of infrared photons at the plane of the object within the boundary box of the object to be  $2 \times 10^5$  photons per second. This photon flux corresponds to an illumination power of  $25\ \text{fW}$ , and an energy deposition on the object of approximately  $100\ \text{pJ cm}^{-2}\ \text{s}^{-1}$ . Figures 2(a) and 2(e) were acquired for a total exposure time of  $30\ \text{s}$  and  $10\ \text{min}$ , respectively, and thus the total energy deposition on the object within the boundary box was  $750\ \text{fJ}$  and  $15\ \text{pJ}$ , respectively. There is an obvious tradeoff between a long exposure time resulting in high image quality and a shorter exposure time with lower energy deposition but resulting in lower-quality images.

Imaging a silicon/gold object, while not being photosensitive itself, demonstrates the low-light imaging capabilities of our system. The conditional nature of our detection scheme, which depends upon the correlated detection of IR and visible photons, reduces our overall quantum efficiency to the order of  $7\%$ , which compares to a quantum efficiency of a leading shortwave infrared low-light camera of  $85\%$ . In terms of dark noise, we measure our detection scheme to have a measured dark noise rate of  $0.01$  noise events per pixel per second, compared with eight noise events per pixel per second from leading shortwave infrared ( $1.5\ \mu\text{m}$ ) low-light cameras [20]. Taking these factors together, we are able to image with higher contrast using a lower illumination power without losing the image in the noise floor of the camera.

In conclusion, we have demonstrated that it is possible to obtain microscope images from visible photons at  $460\ \text{nm}$  by illuminating the object with an equal number of position-correlated infrared photons at  $1550\ \text{nm}$ . To the best of our knowledge, this is the first time ghost imaging has been performed with such a large ratio between signal and idler wavelength, and certainly the first time that this has been combined with an array-type detector. The ability to translate the image information from infrared to visible wavelengths has potential for imaging light-sensitive specimens or where covert operation is desired [21].

**Funding.** Engineering and Physical Sciences Research Council (EPSRC) (EP/I012451/1, K015338/1); European Research Council (ERC) (192382).

**Acknowledgment.** RAK and RHH gratefully acknowledge the staff of the James Watt Nanofabrication Centre at GU for expert support in preparing the imaging test object. RWB acknowledges support by the Canada Excellence Research Chair Program and from the US Defense Threat Reduction Agency.

See Supplement 1 for supporting content.

## REFERENCES AND NOTE

1. S. P. Walborn, C. H. Monken, S. Pádua, and P. H. Souto Ribeiro, *Phys. Rep.* **495**, 87 (2010).

2. T. B. Pittman, Y. H. Shih, D. V. Strekalov, and A. V. Sergienko, *Phys. Rev. A* **52**, R3429 (1995).
3. C. H. Monken, P. H. S. Ribeiro, and S. Pádua, *Phys. Rev. A* **57**, 3123 (1998).
4. J. H. Shapiro and R. W. Boyd, *Quantum Inf. Process.* **11**, 949 (2012).
5. R. S. Bennink, S. J. Bentley, and R. W. Boyd, *Phys. Rev. Lett.* **89**, 113601 (2002).
6. A. Gatti, E. Brambilla, M. Bache, and L. A. Lugiato, *Phys. Rev. Lett.* **93**, 093602 (2004).
7. C. C. Kim and G. Kanner, *Proc. SPIE* **7815**, 781503 (2010).
8. J. C. Howell, R. S. Bennink, S. J. Bentley, and R. W. Boyd, *Phys. Rev. Lett.* **92**, 210403 (2004).
9. S. Karmakar and Y. Shih, *Phys. Rev. A* **81**, 033845 (2010).
10. O. S. Magaña-Loaiza, G. A. Howland, M. Malik, J. C. Howell, and R. W. Boyd, *Appl. Phys. Lett.* **102**, 231104 (2013).
11. R. S. Aspden, D. S. Tasca, R. W. Boyd, and M. J. Padgett, *New J. Phys.* **15**, 073032 (2013).
12. P. A. Morris, R. S. Aspden, J. E. C. Bell, R. W. Boyd, and M. J. Padgett, *Nat. Commun.* **6**, 5913 (2015).
13. V. Studer, J. Bobin, M. Chahid, H. S. Mousavi, E. Candes, and M. Dahan, *Proc. Natl. Acad. Sci. U.S.A.* **109**, E1679 (2012).
14. N. Radwell, K. J. Mitchell, G. M. Gibson, M. P. Edgar, R. Bowman, and M. J. Padgett, *Optica* **1**, 285 (2014).
15. R. W. Boyd and C. H. Townes, *Appl. Phys. Lett.* **31**, 440 (1977).
16. J. S. Dam, C. Pedersen, and P. Tidemand-Lichtenberg, *Opt. Lett.* **35**, 3796 (2010).
17. K. Huang, X. Gu, H. Pan, E. Wu, and H. Zeng, *Appl. Phys. Lett.* **100**, 151102 (2012).
18. G. B. Lemos, V. Borish, G. D. Cole, S. Ramelow, R. Lapkiewicz, and A. Zeilinger, *Nature* **512**, 409 (2014).
19. A. Tosi, D. A. Frera, A. B. Shehata, and C. Scarcella, *Rev. Sci. Instrum.* **83**, 013104 (2012).
20. Princeton Instruments, [http://www.princetoninstruments.com/Uploads/Princeton/Documents/Datasheets/Princeton\\_Instruments\\_NIRvana\\_640\\_LN\\_revN1\\_8-4-15.pdf](http://www.princetoninstruments.com/Uploads/Princeton/Documents/Datasheets/Princeton_Instruments_NIRvana_640_LN_revN1_8-4-15.pdf).
21. The data used to produce the content of this manuscript is available at <http://dx.doi.org/10.5525/gla.researchdata.229>.